Effective Piezoelectric Energy Harvesting Using Beam Plucking and a Synchronized Switch Harvesting Circuit

To cite this article before publication: Hailing Fu *et al* 2018 *Smart Mater. Struct.* in press https://doi.org/10.1088/1361-665X/aac0ba

Effective Piezoelectric Energy Harvesting Using Beam Plucking and a Synchronized Switch Harvesting Circuit

Hailing Fu and Eric M. Yeatman

Department of Electrical and Electronic Engineering, Imperial College London, Exhibition Road, London, SW7 2AZ, United Kingdom

E-mail: h.fu14@imperial.ac.uk and e.yeatman@imperial.ac.uk

Abstract. Piezoelectric energy harvesting, as a way to convert kinetic energy into electricity for low-power electronics, has drawn great attention for the last decade. However, issues still remain, including narrow operating bandwidth and low harvesting capability. In this paper, beam plucking (frequency up-conversion) and a parallel synchronized switch harvesting on inductor (P-SSHI) circuit are integrated in a piezoelectric energy harvester to improve the energy harvesting capability over a wide operating bandwidth. A theoretical model for the plucked beam is established using a distributed-parameter method. In order to study the system dynamics, an equivalent circuit for the plucked beam is built to integrate with the P-SSHI circuit. System dynamics, including the input power, beam tip displacement and output power, are investigated for different driving frequencies and load resistance. The plucked beam provides a uniform and single-frequency vibration for the P-SSHI to generate reliable switching events for any low-frequency wideband vibration; the P-SSHI circuit exhibits an improved electrical damping ratio which is beneficial to alleviating the power fluctuation issue for plucked beams at high frequencies. An experimental validation was conducted, and a close match was obtained. Enhanced output power with low power fluctuation was obtained in the Plucked Beam and P-SSHI circuit (PBPS) configuration over a wide frequency bandwidth with constant load resistance.

Keywords: Piezoelectric, frequency up-conversion, SSHI, beam plucking, equivalent circuit model, broadband, low frequency

Submitted to: *Smart Mater. Struct.*

1. Introduction

In the era of the Internet of Things (IoT), billions of sensing devices will be installed in the environment for the intelligence of everything [1]. However, power supply will be a critical issue which impedes the arrival of this era, as we cannot plug in or replace batteries for all these sensing devices due to the tremendous number. Kinetic energy is widespread in our daily life in various forms, including human motion, fluid

flow, machine operation and structure vibration. Effective harnessing of these energy sources can enable many autonomous and ubiquitous sensing applications [2]. In order to convert kinetic energy into electricity, different conversion mechanisms, including piezoelectric, electromagnetic, electrostatic and triboelectric conversion, have been adopted. Piezoelectric conversion has drawn great attention due to its simplicity in structure and compatibility with micro-fabrication [3].

For piezoelectric energy harvesting, a cantilever beam under base excitation at the transducer's resonant frequency is the typical design. However, it faces the issue of narrow operating bandwidth. For micro-devices, the ideal operating frequency is normally much higher than the available excitation frequencies in practical applications [4], and the devices' performance decreases drastically at off-resonance conditions [5]. Beam plucking (frequency up-conversion), a way to convert low-frequency excitation to high frequency beam vibration, provides a practical solution to harness low-frequency random motions [6, 7]. Different harvesters based on this method have been developed for low-frequency broadband energy harvesting. Pillatsch *et al* developed an inertial motion energy harvester in the form of piezoelectric beam plucking through magnetic coupling with a rotating proof mass. The device had the same size as the Seiko Kinetic wristwatch, and effectively captured low-frequency random excitations [8]. Kathpalia *et al* presented a geometrically nonlinear plucking-based framework for frequency up-converting harvesters [9]. In this design, a stiff bimorph piezoelectric beam was actuated by a flexible nonlinear plectrum undergoing quasi-static loads. Other harvester designs using mechanical impacts [10, 11, 12], magnetic force [13, 14] and non-linear dynamics [15, 16] have also been presented to implement frequency up-conversion for low-frequency random energy harvesting.

However, for plucked beams, when the plucking frequency f_p increases to certain levels, e.g. $f_p > f_n/10$ (f_n is the resonant frequency of the piezoelectric transducer), output power fluctuation occurs due to the fact that the excitation frequency is too high to allow the beam to be fully damped in one excitation cycle. The beam motion interferes with the plucking force, and in some cases, the output power can be reduced due to this interference even when the excitation frequency increases. This phenomenon has been reported in several publications [17, 18, 19]. Fu and Yeatman provided a detailed explanation of the formation of the power fluctuation and its relationship with the resonant frequency of the transducer [19]. Increasing the electrical damping has been suggested as a potential solution to reduce the power fluctuation at high frequencies.

In order to achieve high electrical damping, an effective power management circuit (PMC) is necessary. The standard PMC for piezoelectric energy harvesters is a bridge rectifier in parallel with a storage capacitor [20, 21]. This circuit has the advantage of simplicity and low cost, but also has the issue of low converting capability, i.e. low electrical damping. Different interface circuits have been developed in the last decade in order to improve the power conversion performance [22]. Ottman *et al* developed an adaptive energy harvesting circuit consisting of an AC-DC rectifier with an output capacitor, a switch-mode DC-DC converter and an electrochemical battery

[20]. Experimental results reveal that use of the adaptive DC-DC converter increases power transfer by over 400% as compared to when the DC-DC converter is not used. Synchronized switch harvesting on inductor (SSHI) and synchronized charge extraction (SCE) circuits are two leading piezoelectric energy harvesting PMCs that were developed by researchers from Institut National des Sciences Appliquées (INSA) de Lyon [23, 24]. Improvement from 400% to 900% was predicted using these interface circuits. In these circuits, voltage peak detection and switching circuits are required to reverse the voltage on the piezoelectric beam at beam displacement peaks. Different self-powered switching circuits [25, 26, 27] and improved designs [28, 29, 30] have been developed for SSHI and SCE circuits. E. Lefeuvre *et al.* firstly published a self-powered SSHI circuit with automatic switching based on detection of the peak voltage across the piezoelectric beam [31]. The effectiveness of the SSHI circuit was also verified in the pulsed operation condition [32]. Liang and Liao presented a modified self-powered SSHI circuit using direct peak detection and better isolation among different units [26]. This circuit harvested up to 200% more power than the standard interface circuit. Hehn and Manoli discussed and summarized CMOS circuits for peizoelectric energy harvesting, including efficient power extraction, interface modeling and loss analysis [33]. Wu *et al* developed an efficient self-powered synchronous electric charge extraction CMOS interface circuit dedicated to piezoelectric harvesters [27]. Improvements, including reducing the quiescent current and phase lag of peak detection circuits, were achieved.

For SSHI and SCE circuits, switching events should happen at beam displacement peaks. Determining appropriate switching events is not an issue when the excitation frequency is in a single-frequency harmonic form. This is also the test condition for most of the interface circuits in the above references. However, vibration in the environment is mostly multi-frequency, wideband or even random [34]. The enhancement contributed by the interface circuits is greatly limited when dealing with broadband signals, as the converted energy is subjected to a trade-off between the number of switching events and the squared voltage values at the switching time instant [35]. In order to adapt to broadband excitation cases, Lallart designed a new self-powered SSHI circuit, in which a passive voltage detection circuit was designed to determine appropriate switching events [36]. The original SSHI circuit was only enabled when the voltage on the piezoelectric beam is higher than that on the storage capacitor. Using a similar idea, Shen *et al* designed an adaptive synchronized switch harvesting technique to reduce unnecessary switching events [37].

In this paper, we exploit the beam plucking method to convert the low frequency random input excitation into high and single-frequency beam vibration for the SSHI circuit to generate appropriate and reliable switching events. Meanwhile, the high electrical damping contributed by the SSHI circuit also reduces the power fluctuation issue of plucked beams at high frequencies. To the authors' knowledge, the combination of these mechanisms has not been reported in the literature. In this paper, a system-level integration and analysis is conducted to understand the electromechanical dynamics. An experimental validation was also conducted to verify the theoretical results. This study

provides an effective way to scavenge kinetic energy using piezoelectric conversion for low-frequency wideband input excitation.

2. Theoretical Modelling of Plucked Harvester with SSHI Circuit

2.1. Plucked Energy Harvester using Magnetic Force

Fig. 1 illustrates the schematic of the plucked piezoelectric harvester under tip magnetic excitation. Two magnets, one tip magnet on the beam's free end and one driving magnet on a moving host under the tip magnet, are employed for magnetic plucking. The driving magnet can be carried by any moving host with random and low frequencies, as used, for example, with a miniature air turbine [38] or a wrist-worn motion harvester [39]. The piezoelectric beam is connected to a PMC with a load.

The beam is plucked by the driving magnet once per motion cycle, and then oscillates freely at resonance. The output voltage waveform has a uniform shape and constant oscillating frequency, as shown in the beam vibration curve in Fig. 1(a). The power fluctuation issue happens when the excitation frequency is high. The beam is still vibrating when the second excitation force appears. The vibrating beam affects the work done by the excitation force on the beam, resulting in the power fluctuation. In order to understand the dynamics, a theoretical model is established in this section.

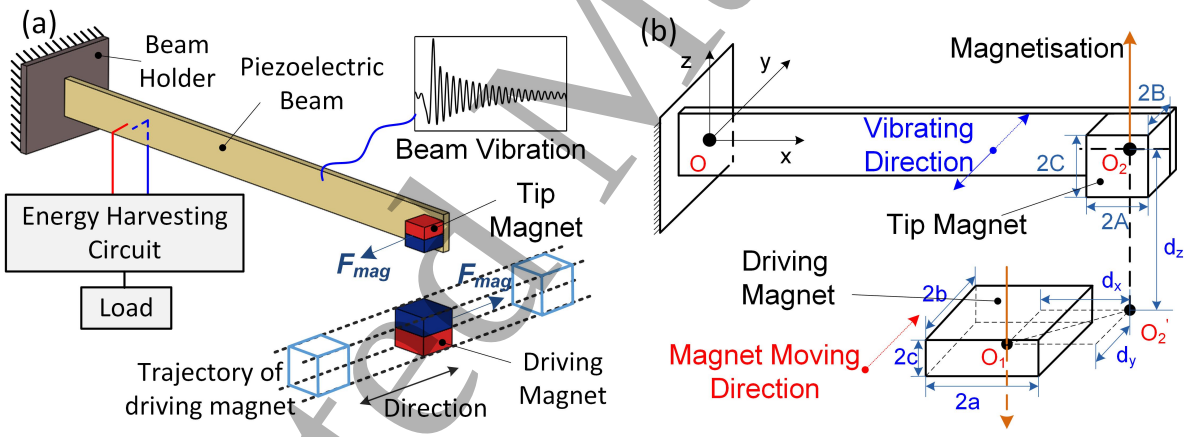

Figure 1. Frequency up-converting harvester using magnetic plucking. (a) Schematic of the harvester and (b) The magnetic plucking model with detailed dimensions.

The magnetic force exerted on the piezoelectric beam is critical for investigating the dynamics. A theoretical model built by Akoun and Yonnet is adopted [40]. The configuration and structural parameters are presented in Fig. 1(b). The magnetic force between two cuboidal magnets in the beam vibrating direction can be calculated using

$$F_{mag}^{y} = \frac{J \cdot J'}{4\pi\mu_0} \sum_{i=0}^{1}\sum_{j=0}^{1}\sum_{k=0}^{1}\sum_{l=0}^{1}\sum_{p=0}^{1}\sum_{q=0}^{1}(-1)^{i+j+k+l+p+q} \cdot \phi_y, \tag{1}$$

where J and J' are the magnet magnetization, μ_0 is the magnetic constant, and ϕ_y is a function of the magnet dimensions and their gaps in 3 axes. The function is given by

$$\phi_y = \frac{1}{2}(U_{ij}^2 - W_{pq}^2)\ln(r - V_{kl}) + \frac{1}{2}rV_{kl} + U_{ij}W_{pq}\tan^{-1}(\frac{U_{ij}V_{kl}}{rW_{pq}}) + U_{ij}Vkl\ln(r - U_{ij}), \quad (2)$$

where

$$U_{ij} = d_x + (-1)^j A - (-1)^i a, \quad (3a)$$
$$V_{kl} = d_y + (-1)^l B - (-1)^k b, \quad (3b)$$
$$W_{pq} = d_z + (-1)^q C - (-1)^p c, \quad (3c)$$
$$r = \sqrt{U_{ij}^2 + V_{kl}^2 + W_{pq}^2}. \quad (3d)$$

These lengths, U_{ij}, V_{kl} and W_{pq}, correspond to the distance between the cube corners and their projections on the axes. The parameters i, j, k, l, p and q, are equal to 0 or 1 according to the specific corner. d_x, d_y and d_z are the gaps between the two magnets in three axes. A, B, C, a, b and c are the dimensions of the magnets, as shown in Fig. 1(b).

Assuming the driving magnet rotates on a revolving host with a radius of r_m at the frequency of ω_h, the gaps between two magnets in three axes can be expressed as

$$d_x = r_m + d_{x0} - r_m\cos(\omega_h t - \alpha_{m0}), \quad (4a)$$
$$d_y = r_m\sin(\omega_h t - \alpha_{m0}) - \upsilon(L_p, t), \quad (4b)$$
$$d_z = d_{z0}, \quad (4c)$$

where d_{x0}, and d_{z0} are the initial gaps along the x-axis and z-axis when the rotor is static, with the driving magnet's angular position $\alpha_{m0} = 0$, $\upsilon(L_p, t)$ is the tip displacement of the piezoelectric beam in the y direction, namely the beam bending direction, L_p is the length of the beam and r_m is the rotational radius of the driving magnet.

For piezoelectric beams under base excitations, Erturk and Inman developed a distributed parameter model [41]. In this paper, the magnetic force applied on the beam's free end is considered to replace the base excitation. Therefore, the mechanical equations of the beam under magnetic plucking at the free end can be written as

$$YI\frac{\partial^4\upsilon(x,t)}{\partial x^4} + c_s I\frac{\partial^5\upsilon(x,t)}{\partial^4 x\partial t} + c_a\frac{\partial\upsilon(x,t)}{\partial t} + m\frac{\partial^2\upsilon(x,t)}{\partial t^2} - \vartheta_r v(t)\left[\frac{d\delta(x)}{dx} - \frac{d\delta(x-L_p)}{dx}\right] = F_{mag}^y(t)\delta(x - L_p), \quad (5)$$

where YI is the bending stiffness, $c_s I$ is the internal damping, c_a is the viscous deformation damping, m is the mass per unit length of the beam, δ_x is the Dirac delta function, ϑ_r is the piezoelectric coupling term in physical coordinates, and $V(t)$ is the voltage on the piezoelectric beam.

Using the method of separation of variables, the beam displacement $\upsilon(x,t)$ can be expressed as a convergent series of the eigenfunctions:

$$\upsilon(x,t) = \sum_{r=1}^{\infty} \phi_r(x)\eta_r(t), \tag{6}$$

where $\phi_r(x)$ and $\eta_r(t)$ are the mass normalized eigenfunction and the modal mechanical coordinate of the cantilever beam with respect to its rth mode shape. The mechanical equation can be further reduced to the modal coordinate by substituting Eq. (6) into Eq. (5), multiplying $\phi_r(L)$ and integrating over the beam length:

$$\frac{d^2\eta_r(t)}{dt^2} + 2\zeta_r\omega_r\frac{d\eta_r(t)}{dt} + \omega_r^2\eta_r(t) - \vartheta_r V(t) = \phi_r(L_p)F_{mag}^y(t), \tag{7}$$

where ζ_r is the modal damping ratio and ω_r is the effective undamped modal frequency of the rth mode shape. The modal damping ratios ζ_r are normally calculated using the logarithmic decrement method from experimentally measured beam displacement curves [42]. The detailed deduction process from Eq. (5) to Eq. (7) can be found in Ref. [41].

The corresponding electrical equation of a piezoelectric beam connected with a PMC is

$$C_p\frac{dV(t)}{dt} + I_l + \sum_{r=1}^{\infty}\vartheta_r\frac{d\eta_r(t)}{dt} = 0, \tag{8}$$

where C_p is the inherent capacitance of the piezoelectric beam and I_l is the current passing through the energy harvesting circuit. The electromechanical dynamics of the harvester can be solved from Eq. 7 and Eq. 8.

2.2. Interface Circuit

2.2.1. Standard Circuit (SC) Fig. 2(a) illustrates a standard regulation circuit to convert the alternating voltage from the piezoelectric beam to a direct form by a bridge rectifier and stored in a capacitor C_s. The power collected on C_s is used to power the load R_l. This circuit has been extensively used in many energy harvester designs as a typical PMC due to its simplicity and low cost.

When the circuit is in a steady state, and the R_lC_s value is much larger than the period of the beam vibration, the voltage V_c on C_s can be regarded as constant. When the voltage from the piezoelectric beam V is lower than V_c, the connection between the capacitor and the piezoelectric beam is blocked by the rectifier, the current I is null. Only when the voltage on the piezoelectric beam is larger than the voltage on the storage capacitor V_c, can the electrical energy be stored for loads. The displacement and output voltage waveforms for Plucked Beam with a Standard Circuit (PBSC) are shown in Fig. 2(b) and (c). In each excitation cycle, only the first several beam vibrations are converted and stored, and then the voltage V is lower than V_c, and the beam operates in the open-circuit condition with a low damping ratio.

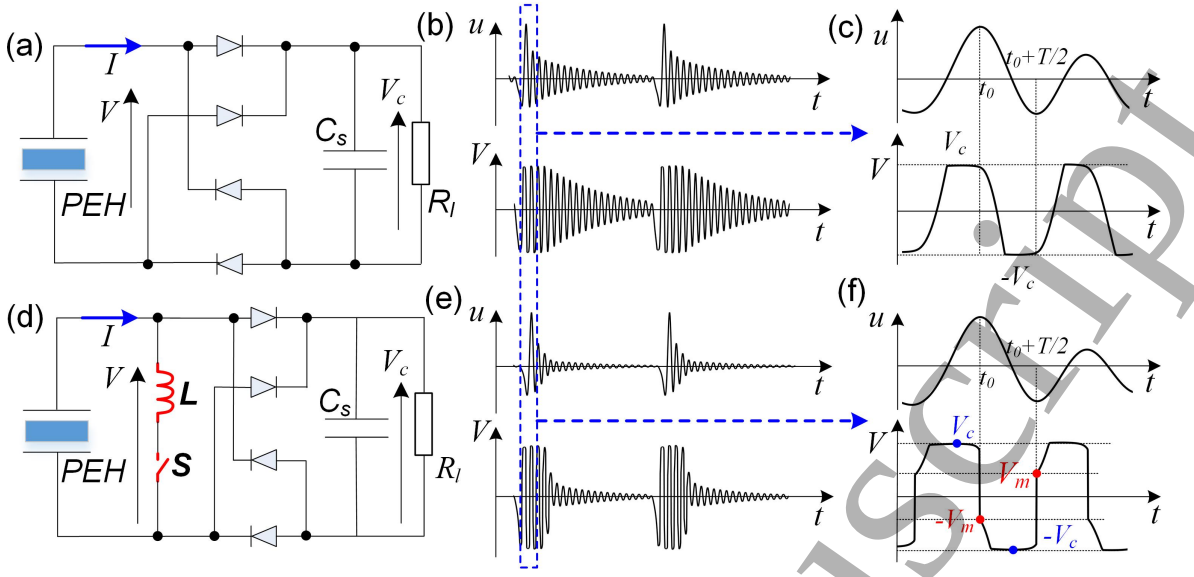

Figure 2. Comparison of the standard ((a), (b) and (c)) and parallel-SSHI ((d), (e) and (f)) circuits for plucked energy harvesters. (a) and (d) Circuit schematics. (b) and (e) Typical displacement and output voltage. (c) and (f) Detailed waveform for the short time frame in (b) and (d).

2.2.2. Parallel-SSHI Circuit For SSHI interface circuits, there are parallel and series types which are all compatible to plucked beams. In this paper, the parallel SSHI (P-SSHI) circuit is adopted, as shown in Fig. 2(d). A switch S and an inductor L are connected in parallel to the bridge rectifier. The switch is controlled by the beam displacement. When beam displacement peaks occur, the switch is closed for a short time frame ($\pi\sqrt{C_pL}$, much shorter than the beam vibration period), and the voltage on the beam is reversed from V_c (or $-V_c$) to $-V_m$ (or V_m), as shown in Fig. 2(f). Then the switch is open, and the voltage on the piezoelectric beam builds up from V_m. A higher voltage V_c can be achieved than that of a SC. Due to the high energy conversion capability of this circuit, the Plucked Beam and P-SSHI circuit (PBPS) configuration exhibits an improved damping ratio, as shown in Fig. 2(e).

To implement the switching control, detection circuits are necessary to monitor displacement peaks. Due to the nature of energy harvesting, self-powered detection circuits have been widely studied to avoid active control. Here, a classical P-SSHI circuit originated from [25, 26, 43] is adopted for the plucked beam, as shown in Fig. 3. There are four main parts: the piezoelectric beam model (equivalent to a current source I_p in parallel to an inherent capacitor C_p), peak detection (PKD) circuits, voltage inverter, and rectification and storage circuit. The PKD circuits are designed to monitor the voltage peaks and to generate switching signals when voltage extrema occur. The switching signal enables the voltage inverter, and the voltage across the piezoelectric beam is reversed by the inductor $L2$ at output voltage peaks. Taking advantage of this self-powered P-SSHI circuit, the remaining parts of this paper investigate the system-level dynamics of a plucked beam with a P-SSHI circuit (PBPS) to achieve effective

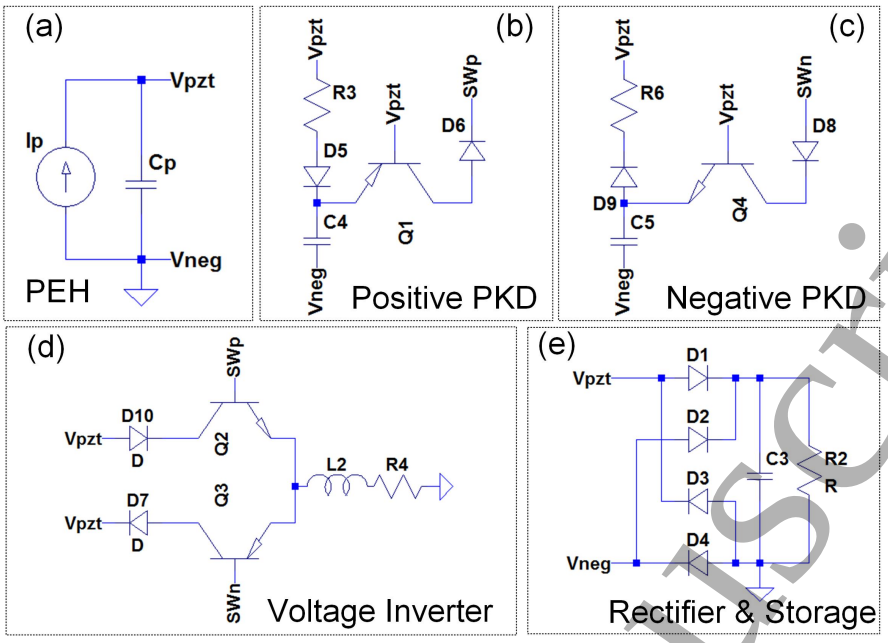

Figure 3. Schematic of the SSHI circuit. The design is divided into 5 blocks based on their functions.

energy harvesting from low-frequency wideband motion sources.

2.3. Equivalent Circuit Model for Plucked Harvester with P-SSHI

In order to study the electromechanical dynamics of the PBPS configuration, a system-level model including beam dynamics and the P-SSHI circuit (shown in Fig. 3) is necessary. In this study, an equivalent circuit model (ECM) for the plucked piezoelectric beam is established using Eq. (7) and Eq. (8). The basic idea is to transfer these equations to equivalent electrical circuits using Kirchhoff's voltage and current laws [44]. Different vibration modes can be considered in the equivalent model to achieve a more precise model when multi-vibration modes are dominant. However, considering the low excitation frequency of plucked harvesters, the first vibration is the dominant mode. Therefore, in this work only the first mode is established in the equivalent circuit.

The equivalent circuit combined with the P-SSHI circuit is shown in Fig. 4. In the ECM, the mechanical module and electrical module are coupled by an ideal transformer, whose turns ratio TR_1 is determined by ϑ_1 in Eq. (7). The electrical components, $R1$, $L1$, and $\frac{1}{C1}$, represent the mechanical damping ratio, the mass and stiffness of the beam, respectively. The applied forces on the beam are equivalent to a voltage source with a gain factor of G_1. In the electrical module, $C2$ is the clamped capacitance of the piezoelectric beam, and the P-SSHI circuit is directly connected to the capacitor $C2$. The components in the equivalent circuit and their corresponding expressions in the theoretical model are listed in Table 1. Using the above model, the dynamics of the whole system can be acquired.

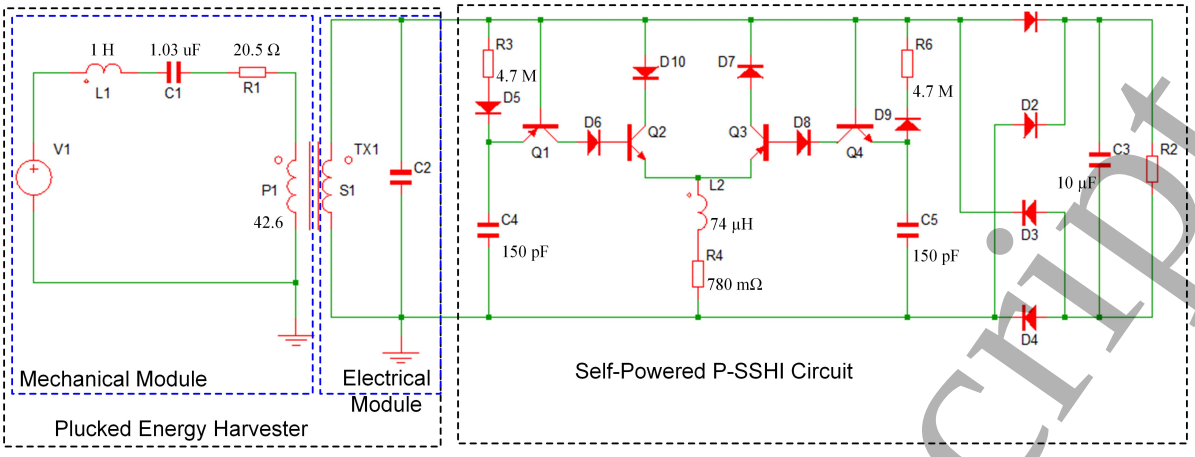

Figure 4. System-level model for plucked energy harvester with a P-SSHI interface circuit. The plucked beam is presented as an equivalent circuit model.

Table 1. Components in the equivalent circuit and their theoretical expressions.

Electrical equivalent	Description of symbols	Mechanical expression
$q(t)$	Charge in the mechanical module	$\eta_1(t)$
$i(t)$	Current in the mechanical module	$d\eta_1(t)/dt$
F_{in}	External forces on the beam	F^y_{mag}
G_1	Voltage gain factor	$\phi_1(L)$
$V1$	Equivalent input voltage	$G_1 \cdot F_{in}$
$R1$	Equivalent mechanical Damping	$2\zeta_1\omega_1$
$C1$	Equivalent stiffness of the beam	$1/\omega_1^2$
$L1$	Equivalent mass of the beam	1
$C2$	Clamped capacitance of the beam	C_p
TR	Turns ratio of Transformer $TX1$	ϑ_1

3. System Dynamics and Analysis

In order to numerically study the system dynamics, a set of design and material parameters are chosen and listed in Table 2. The piezoelectric transducer used in this study was provided by PI Piezo Technology, and the model for the piezoelectric material is PIC 255. The driving magnet is assumed to rotate on a continuously revolving host with a radius of 12 mm. The equivalent circuit in Fig. 4 is implemented in SIMetrix. The equivalent component values listed in Table 1 are calculated in Matlab first and illustrated in Fig. 4 for circuit simulation. The system dynamics of the PBPS combination, including the beam input power, beam displacement and output power for different excitation frequencies and load resistance, are studied and compared to those of the PBSC configuration.

Fig. 5 compares the differences of the electromechanical dynamics of the PBPS and PBSC configurations. As shown in Fig. 5(a) and (b), the driving magnetic forces are the

Table 2. Design parameters of the plucked piezoelectric harvester.

Symbol	Description	Value
$L_p \times b_p$	Beam size	33.5 mm × 1.5 mm
h_p	Thickness of piezo layer	0.1 mm
h_s	Thickness of substrate	0.1 mm
r_m	Magnet rotation radius	12 mm
$a \times b \times c$	Driving magnet size	$0.5 \times 0.5 \times 0.5$ mm^3
$A \times B \times C$	Tip magnet size	$0.5 \times 0.5 \times 0.5$ mm^3
d_{z0}	Initial gap in z-axis	3.2 mm
J	Magnetization of magnets	1.17 T
ρ_m	Density of magnets	7400 kg/m^3
$\bar{e}_{31}$	Piezoelectric voltage constant	-11.3 V · m/N
d_{31}	Piezoelectric charge constant	-180 m/V
ρ_p	Density of piezoelectric material	7800 kg/m^3
ρ_s	Density of substrate material	7850 kg/m^3
Y	Young's modulus of substrate	190 GPa
ϵ_{r33}^T	Relative permittivity constant	1750
s_{11}^E	Elastic constant (compliance)	16.1×10^{-12} m^2/N

same for both cases, whereas the instantaneous input power curves are slightly different due to the different beam vibration velocity affected by the different electrical damping provided by these interface circuits. The benefit of the P-SSHI circuit for plucked beams can be better explained by comparing the difference of the beam tip displacement in Fig. 5(c) and (d). In each excitation cycle, the initial peak-to-peak displacement D_{init} for both cases has marginal difference. However, due to the better energy conversion capability of the P-SSHI circuit, the displacement dampens more quickly than that from a standard circuit with a lower terminal peak-to-peak displacement D_{tml}. This reduced terminal tip displacement is ideal for the plucked beam to avoid the interference between the vibrating beam and the plucking magnetic force. This indicates that the PBPS combination is more likely to be ready for the second plucking motion, especially at high plucking frequencies or multiple driving magnets cases.

Another behaviour from the displacement curve is the two different damping ratios in each plucking cycle. In the first stage (① in Fig. 5), the voltage on the beam is larger than the sum of the voltages V_{C3} on the storage capacitor $C3$ and the voltage drop V_d on diodes. Charges on the beam is transferred to the subsequent circuit, which means both electrical damping and mechanical damping are applied on the beam. When the voltage on the beam is lower than $V_{C3} + V_d$, no charges are stored in the subsequent circuit, and only mechanical damping is effective in this stage (② in Fig. 5).

Due to the better energy conversion capability of the P-SSHI circuit and also the avoidance of the interference between the vibrating beam and the forthcoming driving force, an improved output voltage is acquired on the storage capacitor in Fig. 5(f)

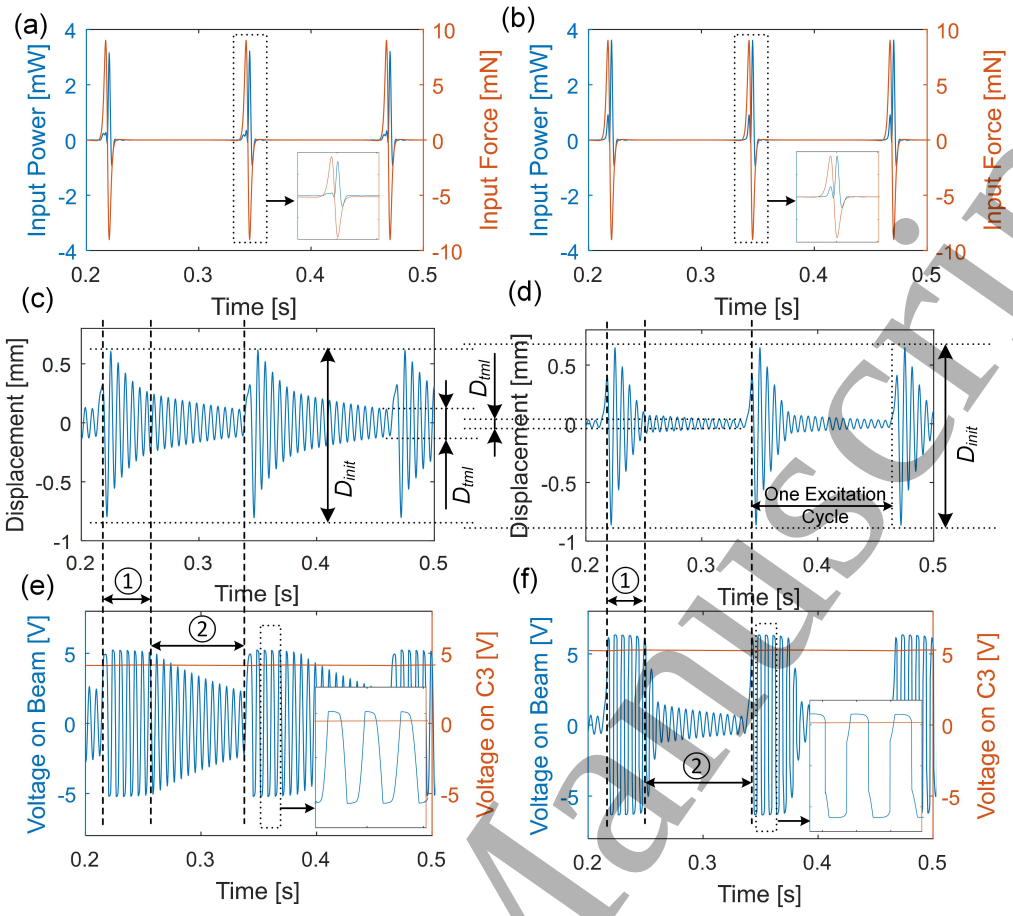

Figure 5. Comparison of the plucked beam with a P-SSHI circuit ((b), (d) and (f)) or with a standard circuit ((a), (c) and (e)) in the steady state. (a) and (b) Instantaneous input magnetic force and input power; (c) and (d) beam tip displacement; (e) and (f) output voltage on the piezoelectric beam and on the storage capacitor $C3$. The input force is the same for both cases, and the plucking frequency is 8 Hz. A 1 MΩ resistor is connected to the storage capacitor $C3$ as the load.

compared to that in Fig. 5(e).

Fig. 6 illustrates the dynamics of the PBPS configuration under random excitation. As shown in Fig. 6(a), the driving frequency varies drastically and randomly from -2 Hz to 16 Hz in the time domain. However, the plucked beam always presents a uniform and single-frequency (resonant frequency) vibration, as illustrated in Fig. 6(b). The plucked beam has successfully converted the random low-frequency to a uniform vibration at resonance. This constant vibration frequency allows the P-SSHI circuit to generate reliable and appropriate switching events for any low-frequency and random excitation, as shown in Fig. 6(c).

In order to examine the performance of the harvesting system in a wider frequency range, the steady-stage output voltage on the storage capacitor versus driving frequency for different resistive loads are simulated and illustrated in Fig. 7. Significant power fluctuation is exhibited for the PBSC configuration, especially at high frequencies, as

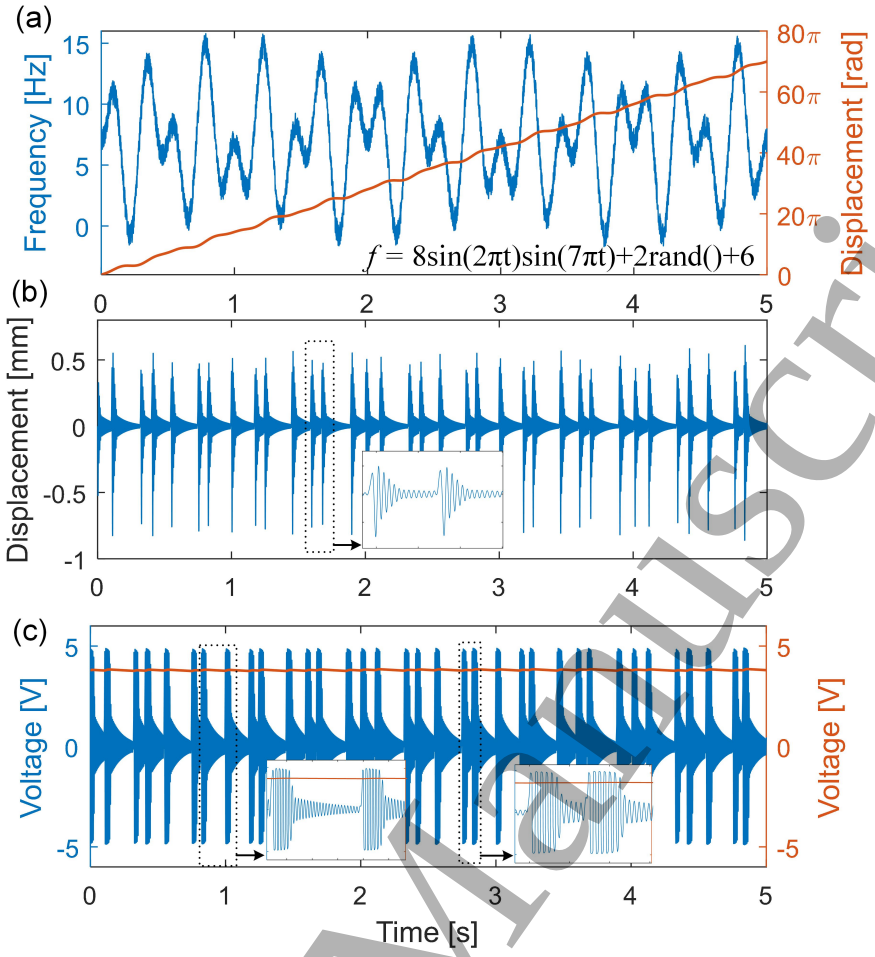

Figure 6. System dynamics of the PBPS configuration under random excitation. (a) Input excitation frequency and angular displacement of the driving magnet; (b) beam tip displacement; (c) output voltage on the plucked beam (blue) and output voltage on the storage capacitor (orange). The function to generate the random driving frequency is given in (a). A 1 MΩ resistor is connected to the storage capacitor $C3$ as the load.

shown in Fig. 7(a). This fluctuation is caused by the interference between the vibrating beam and the subsequent driving force. This interference affects the instantaneous input energy ($P_{in} = F_{mag} \cdot dv(x,t)/dt$) in the beam. Using the P-SSHI circuit, the power fluctuation issue has been reduced to a large extent, as shown in Fig. 7(b). For example, with the load resistance of 2 MΩ, the voltage of the PBSC combination varies from 6.1 V to 9.0 V from 13 Hz to 14 Hz, whereas for the PBPS case, the voltage fluctuation is from 9.4 V to 9.8 V. The enhancement of the performance is mainly contributed by the reduction of power fluctuation and the improved power conversion capability of the P-SSHI circuit.

The power fluctuation frequency corresponds to the resonant frequency of the vibrating beam. This relationship has been discussed by Fu and Yeatman in [19]. The frequency of the i_{th} peak is $f_i = f_n/(n \cdot i)$, where f_i is the frequency of the i_{th} fluctuation peak counting from the resonant frequency f_n downwards. From Fig. 7, the

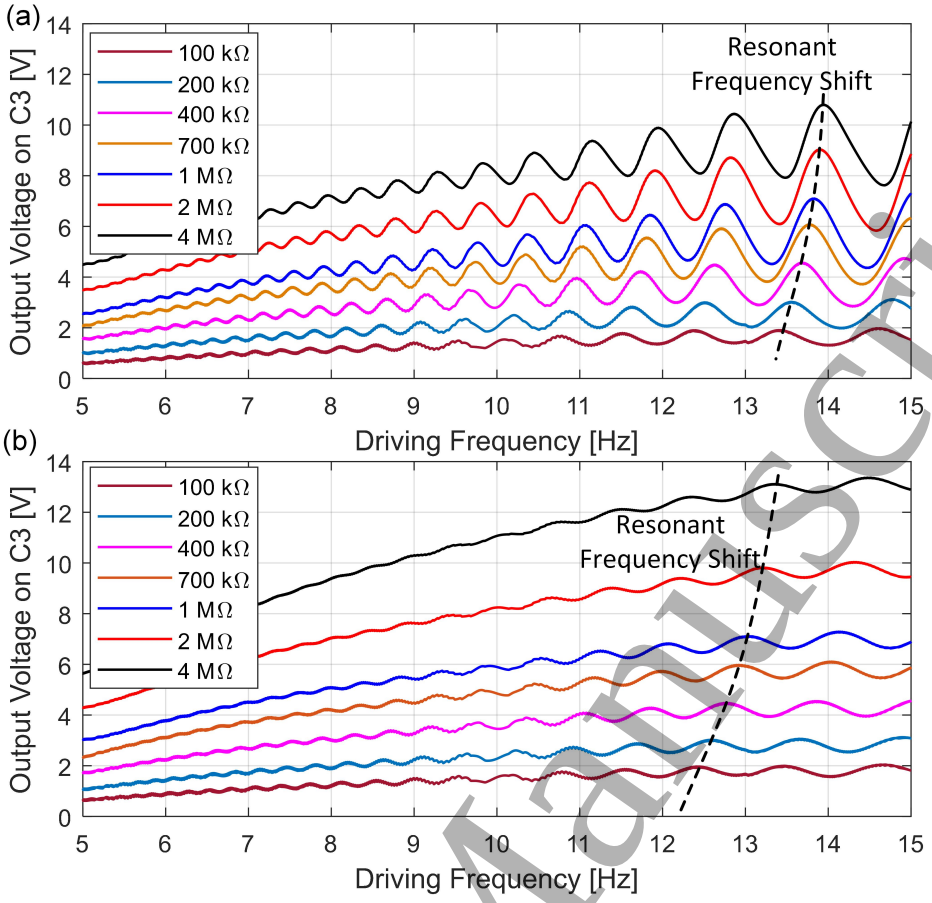

Figure 7. Steady-stage output voltage on the storage capacitor $C3$ versus dirving frequency for different resistive loads. (a) Plucked beam wih the stadard circuit and (b) plucked beam with the P-SSHI circuit.

shift of resonant frequency can be observed from the variation of a particular fluctuation peak for different load resistances. The shift of the resonant frequency occurs due to the different resonant frequencies of piezoelectric beams operating in the short-circuit and open-circuit conditions. According to the theory established by Shu and Lien [45], the relationship of the short-circuit ω_{sc} and open-circuit ω_{oc} resonant frequency is $\omega_{op} = \sqrt{1 + k_e^2} \cdot \omega_{sc}$, where k_e is defined as the system coupling factor. By comparing the shift in Fig. 7(a) and (b), we can state that a larger system coupling factor is obtained in the PBPS case. This improved coupling effect causes the beam to be damped more quickly. As a result, the power fluctuation is reduced at high frequencies.

Fig. 8 depicts the output power as a function of load resistance and driving frequency for both configurations. By comparing the performance in Fig. 8(a) and (b), the advantage of the PBPS combination is further illustrated in terms of reducing the power fluctuation and improving the output performance at high frequencies.

In addition, the maximum output power and the corresponding optimal load resistance are indicated in this figure using red dots. At low frequencies, when the power fluctuation is not significant, the optimal load resistance in both cases can be

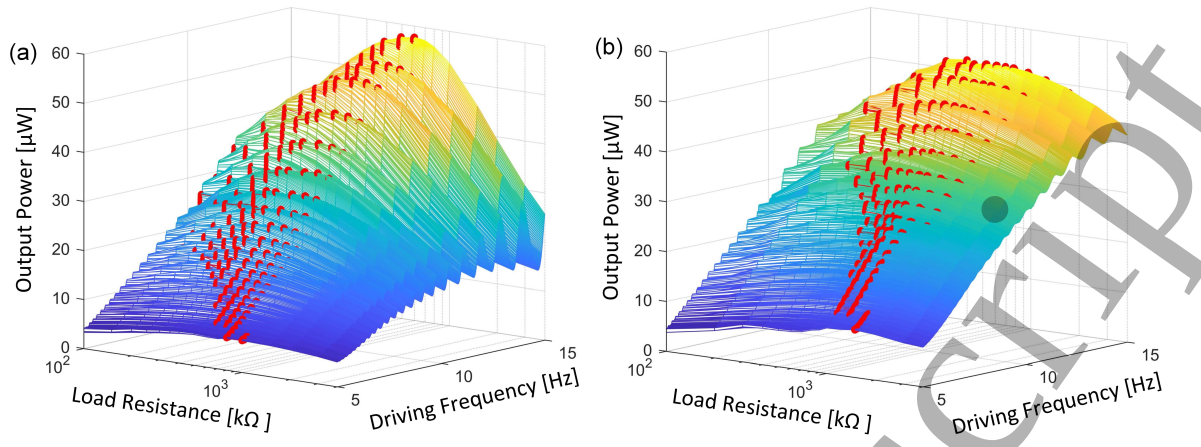

Figure 8. Output power versus load resistance and driving frequency. (a) Harvester with the standard circuit and (b) with the P-SSHI circuit. The red dots on these plots are the maximum output power for a particular driving frequency. These dots also indicate the optimal load resistance for the specific driving frequency.

regarded as constant (600 kΩ for PBSC and 1 MΩ for PBPS). However, when the driving frequency is high, the power fluctuation and the shift of resonant frequency (as shown in Fig. 7) make the optimal resistance vary over a wide range, especially for the case in Fig. 8(a). Therefore, when the harvester operates in a wide frequency range, it is difficult to design a proper load or a subsequent storage circuit with ideal resistance to capture the maximum output power for all frequencies.

Compared to the PBSC case (Fig. 8(a)), the PBPS configuration has better optimal output resistance performance. For example, the maximum output power of the PBSC case varies from 26.0 μW (100 kΩ) to 39.2 μW (500 kΩ) and to 24.6 μW (1.5 MΩ) at 10.67 Hz, 11.01 Hz and 11.34 Hz respectively. For the P-SSHI circuit, the maximum output power varies from 37.0 μW (300 kΩ) to 42.9 μW (700 kΩ) and to 40.6 μW (1.5 MΩ) at 10.86 Hz, 11.19 Hz and 11.48 Hz respectively. The variation of the maximum output power has a less significant variation for the PBPS case (37.0/42.9) than that of the PBSC case (24.6/39.2). Due to the low power fluctuation of the PBPS configuration, as shown in Fig. 8(b), the optimal load resistance can be fixed at a particular value, e.g. 1 MΩ for different frequencies. Therefore, this combination also addresses the issues of optimal load resistance variation for different frequencies.

As in practice, the load resistance for the PMCs is generally fixed for different frequencies, although the maximum output power is not obtained due to the impedance mismatching. Therefore, it is worth investigating the output power performance for constant load resistances. According to the optimal load resistance plots in Fig. 8(a) and (b), The load resistances of 400 kΩ, 600kΩ, 800 kΩ and 1 MΩ are selected for the PBSC case, and 600 kΩ, 800kΩ, 1 MΩ and 1.2 MΩ resistive loads are selected for the PBPS configuration, as shown in Fig. 9. For the PBSC configuration (Fig. 9(a)), although the output power for different load resistances shows marginal differences, the

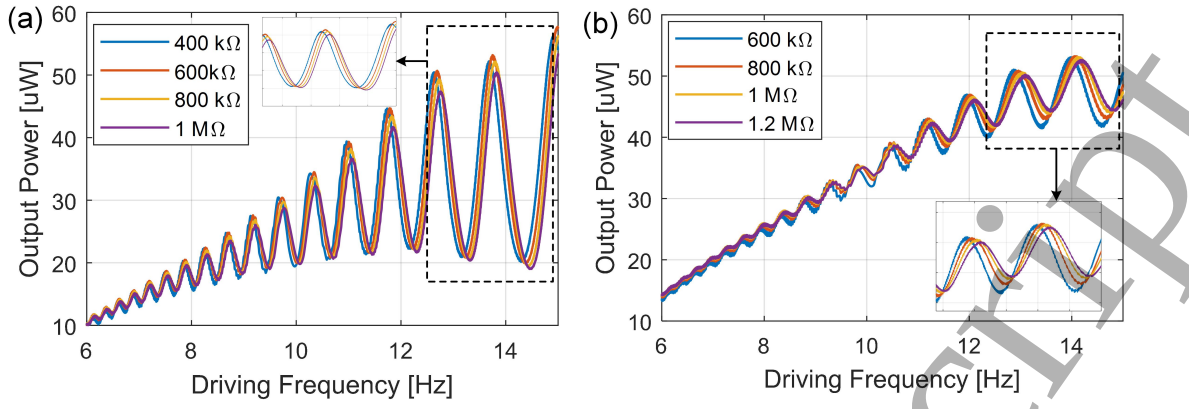

Figure 9. Comparison of average output power versus driving frequency for both configurations with different fixed load resistances. (a) PBSC configuration and (b) PBPS configuration.

output power fluctuates significantly for different driving frequencies, especially at high frequencies. However, for the PBPS combination (Fig. 9(b)), the power fluctuation issue has been largely alleviated for a constant resistive load, and for different load resistances, the performance is quite similar, which means the PBPS configuration also exhibits a wide output impedance range. Hence, the PBPS configuration presents an enhanced output power performance with low power fluctuation for a constant load resistance.

4. Experimental Validation

4.1. Experimental Set-Up

In order to verify the theoretical model and simulation results, an experimental study was carried out. Fig. 10 shows the experimental set-up. Fig. 10(a) illustrates the testing rig for beam plucking. A stepper motor was employed to provide the plucking motion. A driving magnet was mounted on a rotating host fixed on the motor shaft. A piezoelectric beam was placed on a 3-axis positioning stage, so the relative position between the driving and tip magnets can be accurately controlled. A laser displacement sensor was amounted close to the piezoelectric beam to measure the tip displacement.

It is worth mentioning that the stepper motor, 3-axis linear positioning stages and the laser displacement sensor were adopted in this experimental set-up for the purpose of accurate control of the experimental study. For practical applications, the place of the rotating stage is taken by the rotating host structure, e.g. a turbine rotor, and the positioning stages and laser sensor are unnecessary. This plucked harvester can be easily implemented within the dimensions of $\varnothing 35 \times 5$ mm with the gaps between magnets considered. The overall dimensions can be further reduced by miniaturizing the piezoelectric transducer. The output power would be unavoidably reduced for miniaturized devices, but optimized designs using the device space more efficiently could improve the output power.

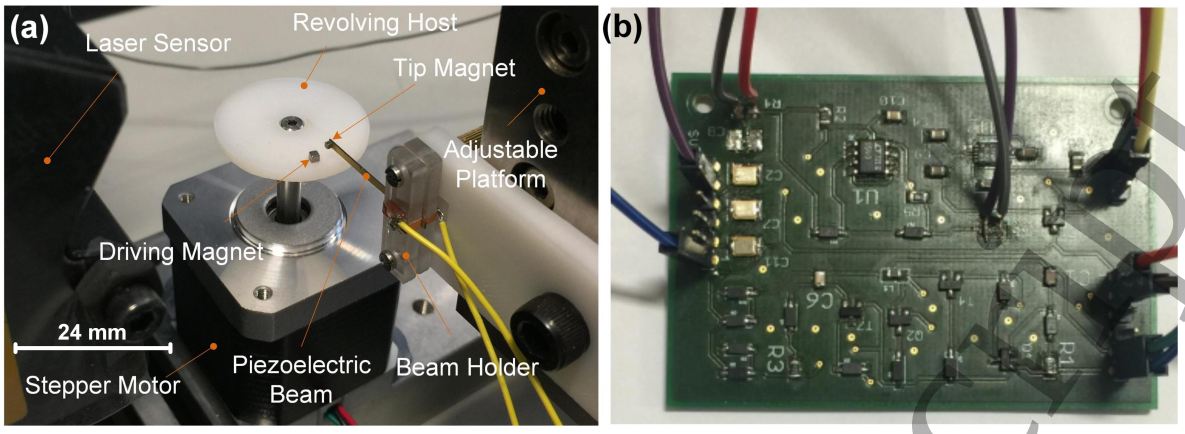

Figure 10. Experimental set-up. (a) Set-up for beam plucking test and (b) P-SSHI circuit implemented on a printed circuit board. The beam dimensions are 33.5 mm × 1.5 mm × 0.2 mm.

The SSHI interface circuit was built on a printed circuit board, as shown in Fig. 10(b). The components and values are the same as those illustrated in the schematic in Fig. 4. The diodes are 1N4148W, and the transistors are MMBT3904 (NPN) and MMBT3906 (PNP). The overall dimensions of the board are 65 × 45 mm. Different resistive loads were connected in parallel to the storage capacitor during the test.

4.2. Results and Discussion

Fig. 11 provides a comparison of the system dynamics for two configurations at 6 Hz both numerically and experimentally. The experimental results fit well with the circuit simulation results in terms of vibration amplitude, frequency and damping ratio. This verifies the validity of the theoretical model and the equivalent circuit model. In addition, for the PBPS combination, the beam vibration and output voltage also exhibit quicker damping rate than that from a standard circuit, as predicted. Two different damping ratios (① and ② in Fig. 11) in one excitation cycle are also illustrated in both experimental and simulated results.

The output impedance for the two configurations was tested and is compared to the circuit simulation results at 6 Hz, as shown in Fig. 12. The simulation results accurately predict the optimal load resistance for both cases (700 kΩ for the PBSC case and 1.2 MΩ for the PBPS case at 6 Hz respectively). Due to the power fluctuation and resonant frequency shift illustrated in Fig. 7, the optimal load resistance is not constant for both cases, which creates a big challenge to extract the maximum power from the harvester at different frequencies. However, the PBPS configuration reduces the power fluctuation issue to a large extent at high frequencies. Therefore, a fixed load resistance, e.g. 1 MΩ, can be used for this configuration to obtain an output power with reasonable losses for varying frequencies.

The dynamics of these configurations for different driving frequencies are depicted in Fig. 13. Again, a close match is achieved between the simulation and experimental

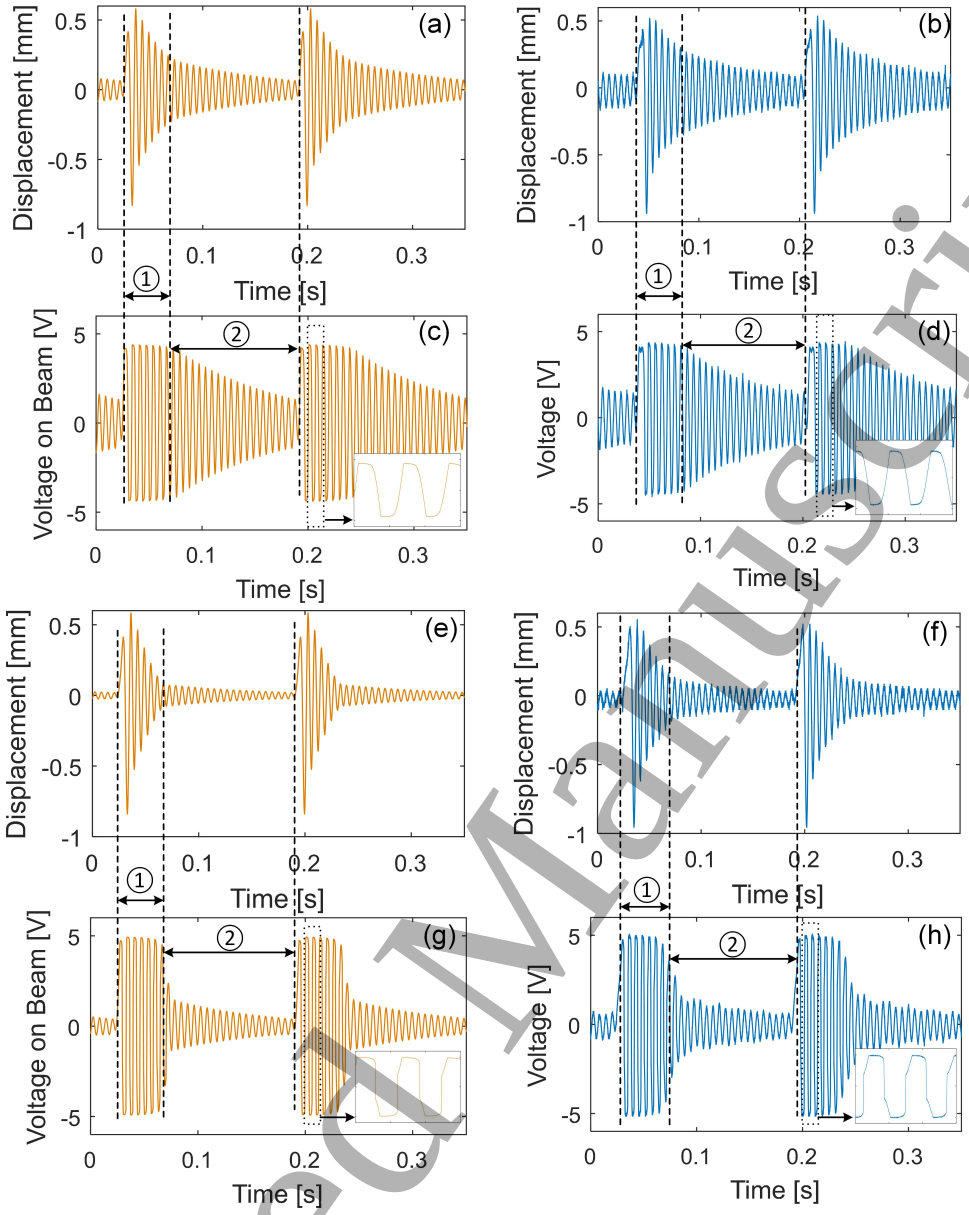

Figure 11. Time domain comparison of beam tip displacement ((a), (b), (e) and (f)) and output voltage ((c), (d), (g) and (h)) on a 1 MΩ resistor at 6 Hz. The first column is circuit simulation results and the second is the experimental results.

results. The power fluctuation issue at high frequencies is illustrated, especially for the PBSC configuration. For the PBPS case, this issue has been alleviated to a large extent. For example, for PBSC, the output power varies from 47.4 μW at 12.75 Hz to 20.5 μW at 13.33 Hz, whereas for PBPS, the power varies from 43.9 μW at 12.47 Hz to 53.2 μW at 13.01 Hz. In addition to the alleviation of the power fluctuation, enhanced output power is also obtained in the PBPS configuration.

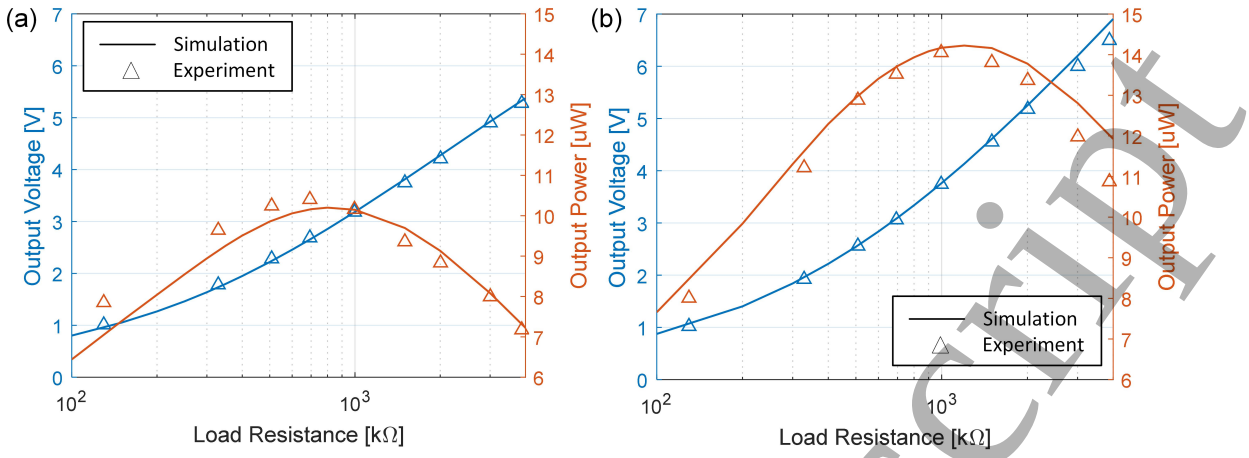

Figure 12. Output impedance curves of two configurations tested at 6 Hz. (a) Plucked beam with the standard circuit and (b) with the P-SSHI circuit.

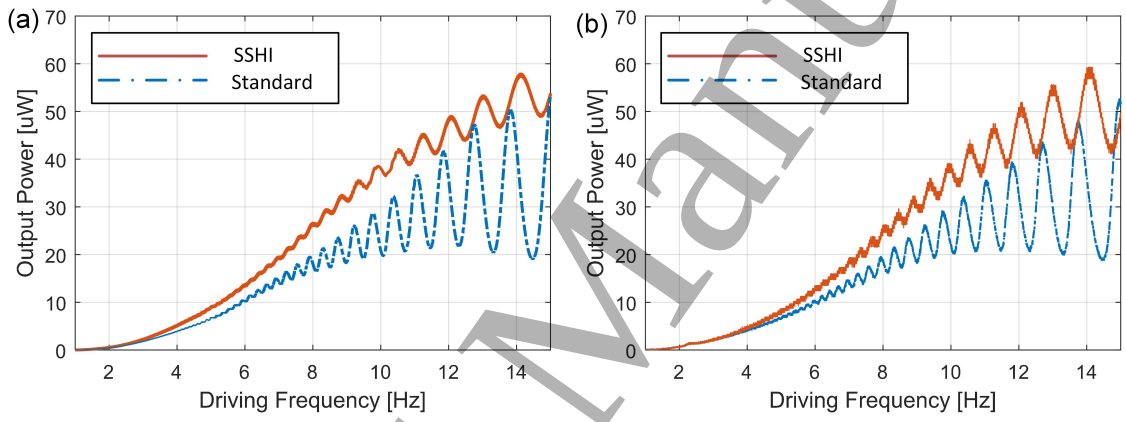

Figure 13. Output power of two configurations versus driving frequency. The resistive load is 1 MΩ. (a) Circuit simulation and (b) experimental results.

5. Conclusions

In conclusion, this paper investigates the combination of the beam plucking method and a P-SSHI circuit for piezoelectric energy harvesting. The plucking method provides a uniform and single-frequency output voltage waveform for the SSHI circuit for peak detection and voltage inversion. The high electrical damping provided by the SSHI circuit also alleviates the power fluctuation for plucking harvesters at high frequencies.

A distributed-parameter model was established for the plucked piezoelectric beam under tip excitation. An equivalent circuit model was built based on the theoretical model in order to study the combination of the plucked beam and a P-SSHI circuit in the system level. The whole system was simulated in SIMetrix. System dynamics, including harvester input power, beam tip displacement, output voltage and output power, were investigated for different load resistance and driving frequency by comparing the differences of the plucked beam with a standard circuit or the P-SSHI circuit.

Both configurations have varying optimal load resistance for different driving frequencies due to the power fluctuation at high frequencies and resonant frequency shift for different resistive loads. However, due to the high electrical damping provided by the P-SSHI circuit, the power fluctuation issue is reduced to a large extent for this configuration, and therefore, the variation of optimal load resistance is not significant compared to the plucked beam with a standard circuit, and fixed load resistance can be used for the plucked beam and P-SSHI configuration for different driving frequencies with reasonable losses in output power. In addition, enhanced output power is obtained in the P-SSHI configuration due to the reduction of power fluctuation of the plucked beam and the high energy conversion capability of the P-SSHI circuit.

An experimental study was carried out to verify the theoretical model and the circuit simulation. The experimental results fit well with the simulation results. Power fluctuation reduction was realized in the P-SSHI configuration with the output power enhanced. This study provides a detailed study and understanding of the combination of the beam plucking method and the P-SSHI circuit. Enhanced output power with low power fluctuation was obtained over a wide frequency bandwidth with constant load resistance.

References

[1] Gubbi J, Buyya R, Marusic S and Palaniswami M 2013 *Future Generation Computer Systems* **29** 1645 – 1660

[2] Briand D, Yeatman E and Roundy S 2015 *Micro energy harvesting* (John Wiley & Sons)

[3] Mitcheson P D, Yeatman E M, Rao G K, Holmes A S and Green T C 2008 *Proceedings of the IEEE* **96** 1457–1486

[4] Jung S M and Yun K S 2010 *Applied Physics Letters* **96** 111906

[5] Zhao L and Yang Y 2018 *Applied Energy* **212** 233 – 243 ISSN 0306-2619

[6] Kulah H and Najafi K 2008 *IEEE Sensors Journal* **8** 261–268

[7] Gu L and Livermore C 2011 *Smart materials and structures* **21** 015002

[8] Pillatsch P, Yeatman E M and Holmes A S 2014 *Sensors and Actuators A: Physical* **206** 178 – 185

[9] Kathpalia B, Tan D, Stern I and Erturk A 2018 *Smart Materials and Structures* **27** 015024

[10] Pozzi M and Zhu M 2011 *Smart Materials and Structures* **20** 055007

[11] Halim M A and Park J Y 2015 *Sensors and Actuators A: Physical* **229** 50 – 58 ISSN 0924-4247

[12] Wei S, Hu H and He S 2013 *Smart Materials and Structures* **22** 105020

[13] Tang Q C, Yang Y L and Li X 2011 *Smart Materials and Structures* **20** 125011

[14] Wickenheiser A M and Garcia E 2010 *Smart Materials and Structures* **19** 065020

[15] Leadenham S and Erturk A 2015 *Smart Materials and Structures* **24** 055021

[16] Barton D A, Burrow S G and Clare L R 2010 *Journal of Vibration and Acoustics* **132** 021009

[17] Xue T and Roundy S 2017 *Sensors and Actuators A: Physical* **253** 101–111

[18] Liu H, Lee C, Kobayashi T, Tay C J and Quan C 2012 *Sensors and Actuators A: Physical* **186** 242–248

[19] Fu H and Yeatman E M 2017 *Energy* **125** 152–161

[20] Ottman G K, Hofmann H F, Bhatt A C and Lesieutre G A 2002 *IEEE Transactions on power electronics* **17** 669–676

[21] Ramadass Y K and Chandrakasan A P 2010 *IEEE Journal of Solid-State Circuits* **45** 189–204

[22] Szarka G D, Stark B H and Burrow S G 2012 *IEEE transactions on power electronics* **27** 803–815

[23] Lefeuvre E, Badel A, Richard C and Guyomar D 2005 *Journal of Intelligent Material Systems and Structures* **16** 865–876
[24] Guyomar D, Badel A, Lefeuvre E and Richard C 2005 *IEEE transactions on ultrasonics, ferroelectrics, and frequency control* **52** 584–595
[25] Lallart M and Guyomar D 2008 *Smart Materials and Structures* **17** 035030
[26] Liang J and Liao W H 2012 *IEEE Transactions on Industrial Electronics* **59** 1950–1960
[27] Wu L, Do X D, Lee S G and Ha D S 2017 *IEEE Transactions on Circuits and Systems I: Regular Papers* **64** 537–549
[28] Lallart M, Garbuio L, Petit L, Richard C and Guyomar D 2008 *IEEE transactions on ultrasonics, ferroelectrics, and frequency control* **55**
[29] Shi G, Xia Y, Wang X, Qian L, Ye Y and Li Q 2017 *IEEE Transactions on Circuits and Systems I: Regular Papers* **PP** 1–14
[30] Lu S and Boussaid F 2015 *IEEE Transactions on Power Electronics* **30** 5364–5369
[31] Richard C, Guyomar D and Lefeuvre E 2005 Self-powered electronic breaker with automatic switching by detecting maxima or minima of potential difference between its power electrodes French Patent, WO2007063194A1
[32] Badel A, Guyomar D, Lefeuvre E and Richard C 2005 *Journal of Intelligent Material Systems and Structures* **16** 889–901
[33] Hehn T and Manoli Y 2014 *CMOS Circuits for Piezoelectric Energy Harvesters: Efficient Power Extraction, Interface Modeling and Loss Analysis* vol 38 (Springer)
[34] Halvorsen E 2008 *Journal of Microelectromechanical Systems* **17** 1061–1071
[35] Guyomar D and Badel A 2006 *Journal of Sound and Vibration* **294** 249–268
[36] Lallart M 2017 *Energy Conversion and Management* **133** 444–457
[37] Shen H, Ji H, Qiu J, Bian Y and Liu D 2015 *Sensors and Actuators A: Physical* **226** 21–36
[38] Fu H and Yeatman E M 2015 *Applied Physics Letters* **107** 243905
[39] Xue T, Yeo H G, Trolier-McKinstry S and Roundy S 2017 A wrist-worn rotational energy harvester utilizing magnetically plucked {001} oriented bimorph pzt thin-film beams *Solid-State Sensors, Actuators and Microsystems (TRANSDUCERS), 2017 19th International Conference on* (IEEE) pp 375–378
[40] Akoun G and Yonnet J P 1984 *IEEE Transactions on Magnetics* **20** 1962–1964
[41] Erturk A and Inman D J 2011 *Piezoelectric Energy Harvesting* (John Wiley & Sons, Ltd)
[42] Pillatsch P, Yeatman E and Holmes A 2013 *Smart Materials and Structures* **23** 025009
[43] Wu Y, Badel A, Formosa F, Liu W and Agbossou A 2014 *Journal of Intelligent Material Systems and Structures* **25** 2165–2176
[44] Yang Y and Tang L 2009 *Journal of Intelligent Material Systems and Structures* **20** 2223–2235
[45] Shu Y and Lien I 2006 *Smart materials and structures* **15** 1499